

Turonian Oceanic Red Beds in the Eastern Alps: Concepts for palaeoceanographic changes in the Mediterranean Tethys

S. Neuhuber^{a,*}, M. Wagneich^a, I. Wendler^b, C. Spötl^c

^a *Universität Wien, Department für Geodynamik und Sedimentologie, Althanstrasse 14, 1090 Vienna, Austria*

^b *Universität Bremen, Fachbereich 5 - Geowissenschaften, Postfach 330440, 28334 Bremen, Germany*

^c *Leopold-Franzens-Universität Innsbruck, Institut für Geologie und Paläontologie, Innrain 52, 6020 Innsbruck, Austria*

Received 3 July 2006; received in revised form 28 March 2007; accepted 29 March 2007

Abstract

Several transitions of Lower to Middle Turonian pelagic marl–limestone–cycles into Oceanic Red Beds were studied at high resolution to gain a better understanding of the Tethyan marine system before and during red bed initiation and development. Samples were analysed for mineralogy, geochemistry, and stable isotope composition. In particular, carbonate geochemistry of diagenetically largely unaltered calcite was used to explore palaeoceanographic changes in the western Tethys. Principal component analysis of carbonate chemical data showed that the development of red coloured pelagic sediments is accompanied by a shift towards highly oligotrophic conditions in the surface ocean as well as a decrease in hydrothermal activity. The formation of red beds is most likely associated with a shift towards more oxic conditions in basins with black shale deposits that eventually resulted in enrichment of thiophile elements in the entire basin. Depletion in nutrients (most likely phosphate) and red bed deposition followed the maximum flooding in the Early Turonian. Highly productive marsh areas from the proximal European shelf were reworked and supplied nutrients during transgression. A gradual nutrient depletion during sea level highstand might be the cause of significantly diminished nutrient availability. Carbonate production in this low latitude setting was influenced by orbital variation in insolation (20 ka cycle). Stable carbon isotope stratigraphy reveals low sedimentation rates (between 1 and 7 mm/kyr) and a duration of episodes of Cretaceous oceanic red bed deposition between 30 and 360 kyrs.

© 2007 Elsevier B.V. All rights reserved.

Keywords: CORB; Turonian; Carbonate chemistry; Stable isotope stratigraphy

1. Introduction

Cretaceous oceanic red beds (CORB) are a well-known phenomenon in Upper Cretaceous pelagic sediments and widespread occurrences are reported from the lower Turonian onward (Melinte and Jipa, 2005; Wang

et al., 2005; Hu et al., 2005a,b). Before Turonian times, more regionally restricted episodes of red bed deposition are known (e.g. Hu et al., 2005a,b). Red coloured pelagic sediments of varying carbonate content are exposed in the entire Tethys area and in parts of the Atlantic and the Pacific (for a summary see Wang and Hu, 2005). Most authors attributed the simultaneous onset of CORB deposition in the Turonian to a fundamental change in the oxidation state of the ocean, which reflects changes in the

* Corresponding author.

E-mail address: stephanie.neuhuber@univie.ac.at (S. Neuhuber).

circulation and the carbon budget of the ocean (e.g. Wang et al., 2005) and followed the period of extensive mid-Cretaceous black shale deposition.

The palaeoceanography of the Mediterranean Tethys (Fig. 1) in the Turonian is dominated by a clockwise gyre (Poulsen et al., 1998), which transported water masses along the northern margin of the basin in an eastward direction and was supplied mainly by a westward current along the African shelf. Nd isotope measurements attest to an increased Pacific influence in the surface waters of the eastward current from the Albian onward (Puceat et al., 2005) where the successive opening of North and South Atlantic ultimately strengthened this current (Puceat et al., 2005). Small-scale circulation between different terranes in the central western Tethys was most likely highly variable due to rapid palaeogeographic changes. The sea level reached its maximum in the early Turonian (Gradstein et al., 2004) when pelagic sediments covered most of the European shelf. Autochthonous Middle to Upper Cretaceous deposits from the proximal shelf of Europe record this transgression where Lower Turonian glauconitic sands cover salt marsh facies (Fuchs et al., 1984).

This paper focuses on a pelagic section of the Ultrahelvetetic passive margin of Europe with several tran-

sitions into CORBs on a small temporal scale. The sediments were deposited above the Cretaceous calcite compensation depth (CCD), which was not significantly different from today's CCD (between 4500 and 5500 m bsl) (Tyrrrell and Zeebe, 2004). The sedimentation rate and the degree of organic carbon preservation were relatively low. The section covers the Lower to Middle Turonian with several red marl–limestone intervals.

Mineralogy, bulk geochemistry of selected samples, carbonate geochemistry, and stable isotope distribution were studied at a high resolution to gain a thorough understanding of the marine system before and during CORB initiation and development. A total of 51 samples were analyzed for geochemistry, stable carbon and oxygen isotopes. Additionally, the mineralogy of 23 marl beds was determined. The emphasis of this study lies in the carbonate geochemistry of diagenetically largely unaltered calcite that was used to track palaeoceanographic changes in the Mediterranean Tethys. Because limestone–marl alternations are prone to differential diagenesis (e.g. Melim et al., 2002), the degree of diagenetic alteration is crucial for a sound interpretation of geochemical data. We used Mn/Sr and $\delta^{13}\text{C}$ values that are sensitive to diagenetic overprint (Jacobsen and Kaufman, 1999).

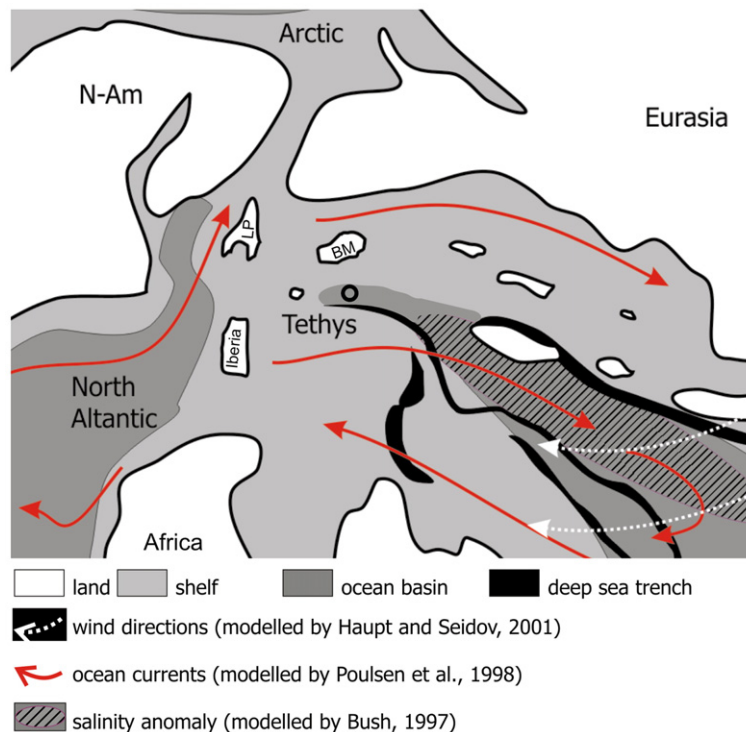


Fig. 1. The Turonian (94 Ma) paleogeography (www.scotese.com), circulation systems and wind systems. Circle indicates location of the Buchberg profile. BM: Bohemian Massif; LP: London Platform.

We further compare carbon isotope data of the Buchberg profile to the dated composite chalk curve of Jarvis et al. (in press) and to the Contessa profile in Italy (Stoll and Schrag, 2000) for high-resolution stable isotope stratigraphy. This enabled us to calculate sediment accumulation rates as well as the duration of individual CORB episodes.

2. Geology and stratigraphy

Helvetic and Ultrahelvetic units of the Eastern Alps of Austria and Bavaria record the sedimentation at the northern continental margin, i.e. the shelf and continental slope to the north of the Penninic–Ligurian Ocean or the Alpine Tethys (e.g. Faupl and Wagneich, 2000; Stampfli et al., 2002). Ultrahelvetic units of the Eastern Alps to the east of the city of Salzburg are preserved in highly deformed tectonic slices within the Rhenodanubian Flysch Zone. The Buchberg section is situated in one of these slices, west of Lake Attersee and east of the village of St. Georgen im Attergau, at the northern slope of the Buchberg hill (Fig. 2). The section crops out in a small southwest–northeast flowing creek (WGS 84 coordinates: 13° 31'45" E; 47° 56' 04" N).

The section exposes a Cenomanian–Turonian succession of limestones, marly limestones, and marlstones where the Cenomanian is partly covered. Light grey limestones with dark grey mottles alternate with medium and dark grey spotty marlstones at the base of the section. Grey and red limestones and marlstones of Turonian age follow. At the top Ultrahelvetic rocks are covered by

sandstone debris of the Rhenodanubian Flysch Zone where the Flysch is overthrust onto Ultrahelvetic rocks.

The stratigraphy of the profile is based on planktonic foraminifera and nannofossils. Nannofossil standard zones CC10 to CC12 (Perch-Nielsen, 1985; UC6b–UC8a of Burnett et al., 1989) have been identified in the profile (Fig. 3). The investigated part of the section with continuous exposure starts above the Cenomanian–Turonian boundary interval. The transition into the first red marl lies within zone CC11/UC7, above the first occurrence of *Quadrum gartneri*. The top of the section was dated to the middle Turonian (zone CC12/UC8a), based on the first occurrence of *Eiffelithus eximius*. An early to middle Turonian age is also established by the presence of the planktonic foraminifer *Helvetoglobotruncana helvetica*.

The section consists of alternating limestone–marl cycles with four transitions of grey coloured intervals into red beds (Fig. 3). In the lower part of the profile, the red colour is restricted to marl beds whereas both marl and limestone beds at the top are of red colour. The beds have even or wavy planes and tend to be more bioturbated at the top of the profile. Compared to all other CORB intervals, the first interval (3.7 m–3.95 m) is more brownish in colour. The second CORB between 3.77 m and 3.95 m is rather thin (17 cm) and the red colour is restricted solely to marl beds. The red marls and limestones of the third CORB interval (4.55 m–4.95 m) are bioturbated and the bioturbated zones are grey. This interval is separated from the fourth CORB (5.15 m–6.25 m) by one thick grey limestone bed. The

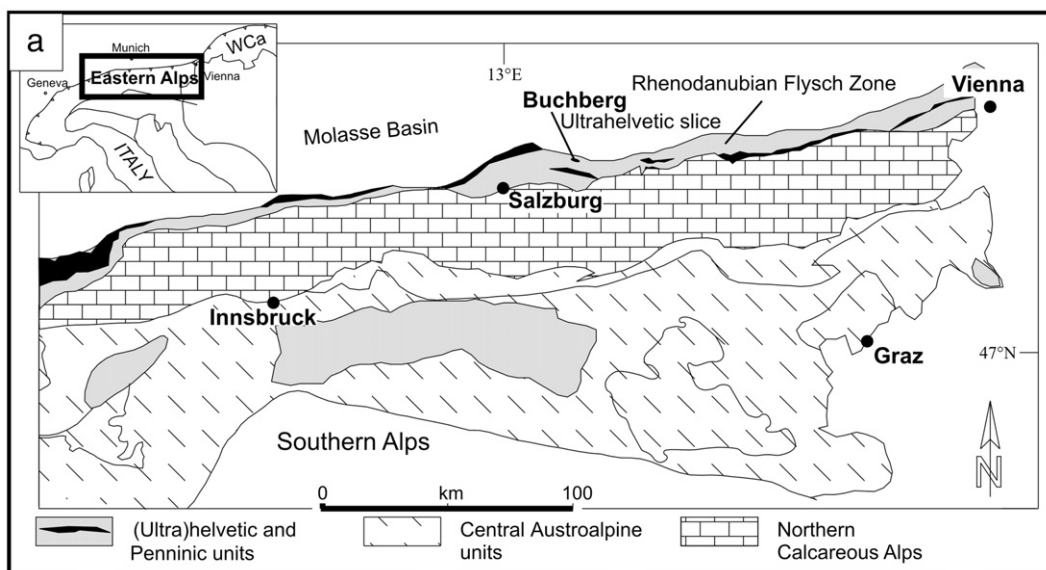


Fig. 2. Location and geologic setting of Buchberg; overview of location of Eastern Alps (a), WCa = West-Carpathians.

uppermost CORB is the most prominent and spans an interval of about 1.1 m including red marls and bioturbated red marly limestones. The transition to the last red marl bed is covered.

3. Materials and methods

3.1. Field work and sample preparation

The central part of the section was excavated and sampled on a bed by bed scale with sample intervals

between 5 and 30 cm. Calcite veins with stylolites are uncommon in the profile. Those parts were omitted for geochemical analysis as they indicate tectonic deformation most likely accompanied by geochemical alteration. The stratigraphic section was compiled with StratDraw (Hoelzel, 2004).

A total of 58 samples were split for palaeontological and geochemical analyses. Samples were ground in an agate mill to a fine powder for mineralogy, bulk and carbonate geochemical analyses, as well as for stable isotope analysis.

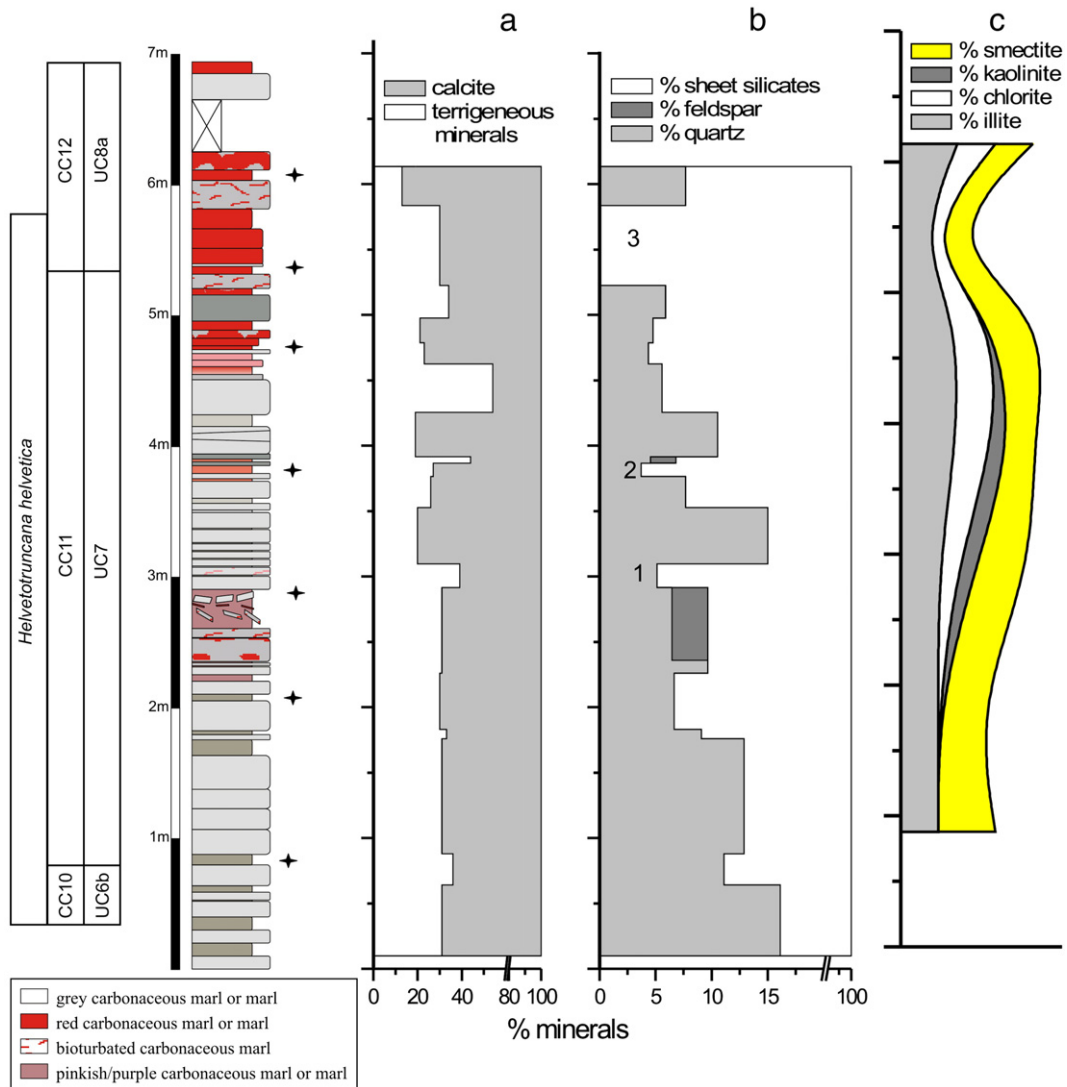


Fig. 3. Biostratigraphy and mineralogy of the Buchberg section. Protruding beds indicate beds with higher carbonate content. White beds: grey marls/limestones; grey beds: red marls/limestones; mottled beds indicate strong bioturbation. Nannofossil biozonations of Perch-Nielsen (1985:CC) and Burnett et al., 1989:UC); zone CC12 is defined by the first occurrence of *Eiffelithus eximius*. Vertical step graphs of the mineralogical composition of marl beds: distribution of terrigenous (sum of sheet silicates, quartz, and feldspar) vs. marine derived mineral (calcite) (a); distribution of terrigenous minerals (sheet silicates, quartz, and feldspar) in the section: numbers 1–3 indicate sheet silicate maxima (b); Qualitative clay mineral distribution: stars next to beds specify position of clay mineral samples (c).

3.2. Bulk and clay mineral analysis

Semiquantitative X-ray diffractometry (XRD) analysis resolved the mineralogical composition of marls (Schultz, 1964). Clay mineral composition of 7 marls was measured on the sieved 63–160 μm fraction (Fig. 3). Carbonate aggregates of this fraction were dissolved in 0.1 M EDTA and the remaining insoluble residue was rinsed with deionized water and saturated in 1 M KCl and 1 M MgCl_2 , respectively. The use of this fraction ensures no influence of weathered material. Both slides were subsequently treated with ethyleneglycol (for 12 h at 60 $^\circ\text{C}$) and heated to 300 and 500 $^\circ\text{C}$. All diffraction patterns were recorded with a Philips X-ray diffractometer with PW 1830 generator ($\text{Cu K}\alpha$) using an acceleration voltage of 45 kV and a current of 35 mA.

3.3. Carbonate and organic carbon content

The carbonate content of all samples was investigated by acidification and liberation of carbon dioxide (ÖNORM L1084) with a standard deviation of 5%. The results from semiquantitative XRD analysis and the carbonate determination show good agreement. A Leco

Multiphase Carbon Determinator LECO RC-412 was used to measure the content of total organic carbon (TOC) at 550 $^\circ\text{C}$ and an afterburner temperature of 800 $^\circ\text{C}$.

3.4. Bulk geochemistry

Bulk geochemistry was measured on powder pills with a sequential wavelength disperse X-ray fluorescence spectrometer (Spectro X-Lab 2000) with Pd-anode calibrated to the SARM 46 standard (Pretoria, Republic of SA). The analytical uncertainty is below 5% for major elements and between 5 and 10% for trace elements.

3.5. Geochemistry of the carbonate fraction: acetate extraction

This extraction procedure essentially follows the extraction for carbonate bound heavy metals first described by Tessier et al. (1979) and releases carbonate bound elements as well as ions sorbed to mineral surfaces such as clays, oxides, and sulfides (Sulkowski and Hirner, 2006). Well-crystallized oxides are not affected by this procedure (Tessier et al., 1979; Sulkowski and

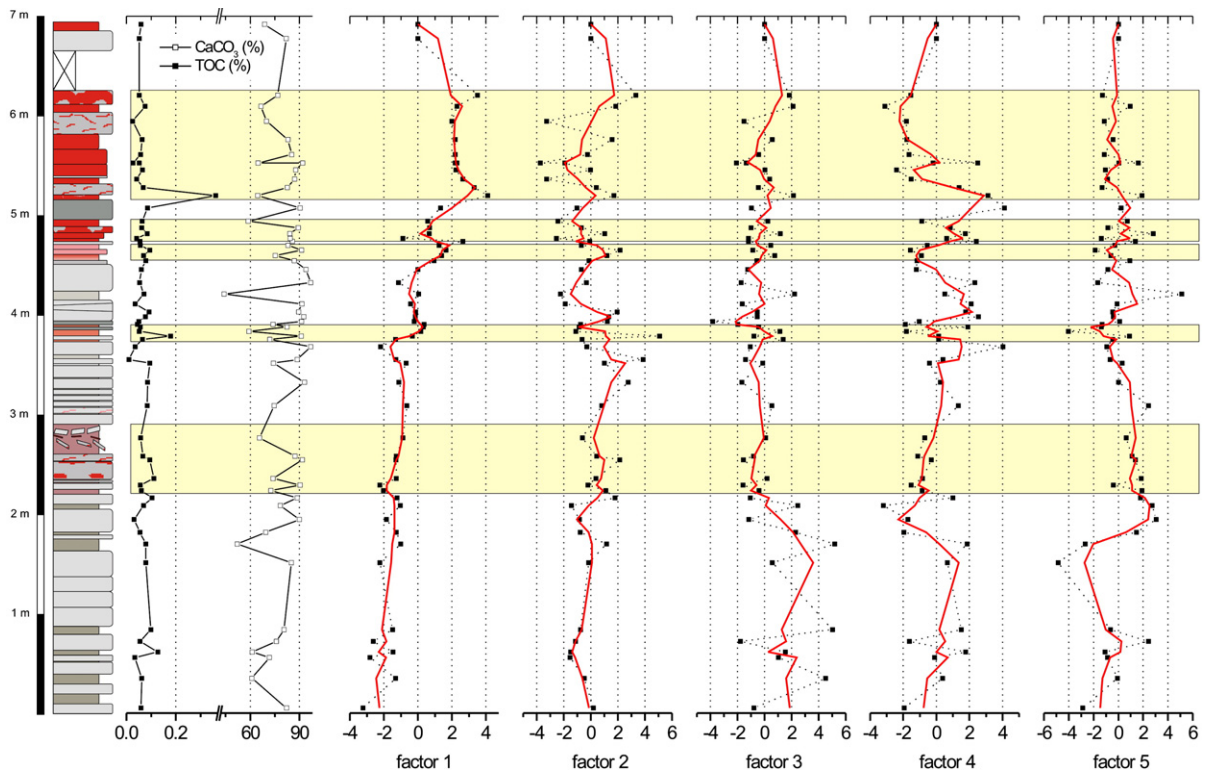


Fig. 4. TOC and carbonate content of the Buchberg profile (two left graphs); factor analysis of the five factors of the acetate extractable fraction (x-axis); for loadings and variation explained by each factor see Fig. 7. The grey bar indicates the position of CORBS in the section.

Hirner, 2006). This is supported by the presence of hematite in the XRD patterns after acetate treatment of samples from a different location with higher hematite content. Each 0.5 g sample was dissolved in 10 ml 1 M acetic acid buffered to pH 5.5 with 2 M Na acetate to guarantee complete carbonate dissolution. The high Na concentration in the buffer solution ensured that re-adsorption of ions was limited. After CO₂ release, the samples were agitated over night. Low amounts of additionally released CO₂ were removed by opening the tubes and were subsequently shaken for another 2 h. The solution was centrifuged, diluted, and acidified with HNO₃ for ICP-MS analysis (Elan 6100 Sciex). Ca and Mg were additionally determined by DCP-OES (Spectraspam IIIB Emission Spectrometer). The carbonate-free residue was washed twice with deionized water, dried at 80 °C, weighed, and compared to the results of the carbonate measurements. All reagents were of analytical grade and the reaction vessels were washed in

2 M HCl and rinsed with deionized water before use. Reference materials GSR2, AGV1, and SDC1 were used to track the accuracy of measurements. The analytical reproducibility for Mg, Al, P, V, Cr, Fe, Mn, Co, Ni, Cu, Zn, Rb, Sr, Ba, and Pb is below 4% (RSD) and between 4 and 9% for Cd, Ti, and U, which are closer to the detection limit. For DCP analysis the analytical reproducibility of triplicate measurements is within 5%.

3.6. Stable carbon and oxygen isotopes

Stable carbon and oxygen isotope compositions of bulk samples were determined using a ThermoFinnigan DeltaPulsXL mass spectrometer equipped with a Gas-Bench II following the procedure described in Spötl and Vennemann (2003). Results are calibrated against NBS 19, CO1, and CO8 standard reference materials and are reported on the VPDB scale.

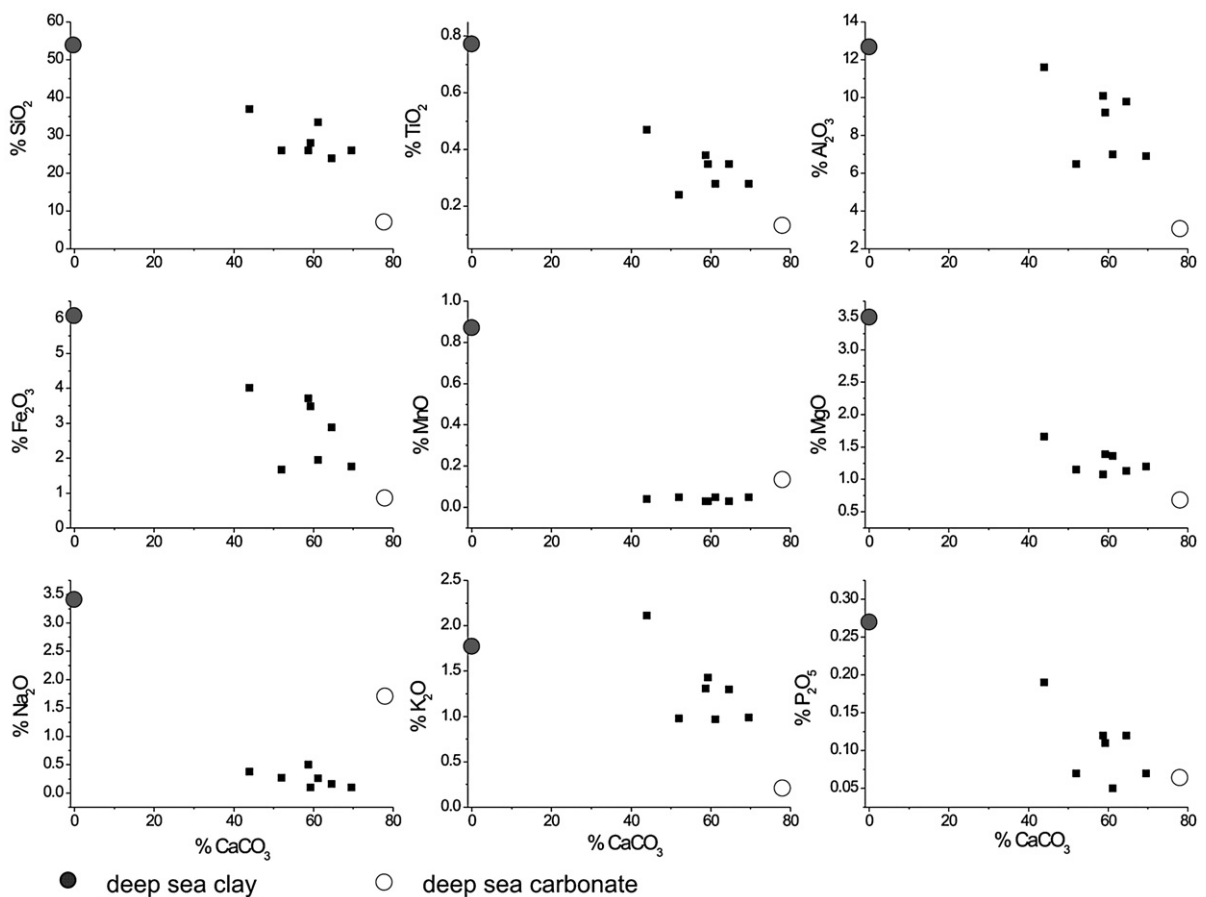


Fig. 5. Comparison of average deep-sea carbonates and average shale composition (Turekian and Wedepohl, 1961) to bulk geochemical analysis (XRF) of Buchberg.

3.7. Principal component analysis

Prior to principal component analysis (PCA) the dataset was tested for homogeneity by cumulative distribution function (CDF) diagrams (Reimann et al., 2001). All geochemical data were examined by PCA. The statistics program SPSS computed factors by Quartimax rotation with Kaiser normalization. Factors from geochemical analysis were then compared to the other variables i.e. mineralogy, stable isotope values, and TOC.

4. Results

4.1. Bulk and clay mineralogy

In general, an overall change in source area, ocean circulation, or aeolian dust flux can be detected more readily from XRD bulk mineralogical data of marl layers with a higher input of land derived detritus than from limestone layers where the terrigenous signal is strongly diluted by the biological carbonate production. For this reason we analyzed the bulk mineralogy of marl layers only.

The amount of calcite and terrigenous minerals (Fig. 3) in the lower 3 m are fairly constant and start to fluctuate a little above the first CORB. 85% of the terrigenous fraction consists of phyllosilicates, which indicate a distal depositional setting. In the land-derived fraction (i.e. phyllosilicates, quartz, and feldspar), three maxima in phyllosilicates are found at 3 m, below 4 m, and below 6 m (Fig. 3b). Mineralogical data suggest a gradual increase in silicates, which precede all maxima. CORBs appear in regions with a higher content of phyllosilicates (Fig. 3b). Two samples contained plagioclase.

The clay mineralogy was interpreted qualitatively only (Fig. 3c). In two samples (Bu 6 and Bu 18) the K-saturated sample did not collapse to 10 Å but remained at 12 Å, which indicates a low-charged smectite. Therefore two kinds of smectitic clay minerals — a high and a low charged smectite — are present in these samples.

Chlorite was found in all but the first sample. Low amounts of kaolinite are present in the central part of the profile between 3 m and 4 m. In all red-coloured marls an additional 12 Å clay mineral phase (Na saturation) — most likely vermiculite — was identified.

4.2. Carbonates and organic carbon content

The CaCO_3 content lies between 43 and 98 wt.% and the TOC varies between 0.01% and 0.36%. Three dis-

tinct spikes in TOC are linked to marl layers (Fig. 4). The dominant C sink is biogenic carbonate whereas the organically bound C lies in the permil range of the total carbon content. The only carbonate phase detected by XRD is calcite and its content is on average highest in the central part of the profile between 250 and 550 cm.

4.3. Bulk geochemistry

Bulk geochemical (XRF) data of 7 marls and limestones were compared to average values for deep-sea carbonates and deep-sea clays (Turekian and Wedepohl, 1961) where most concentrations are located between

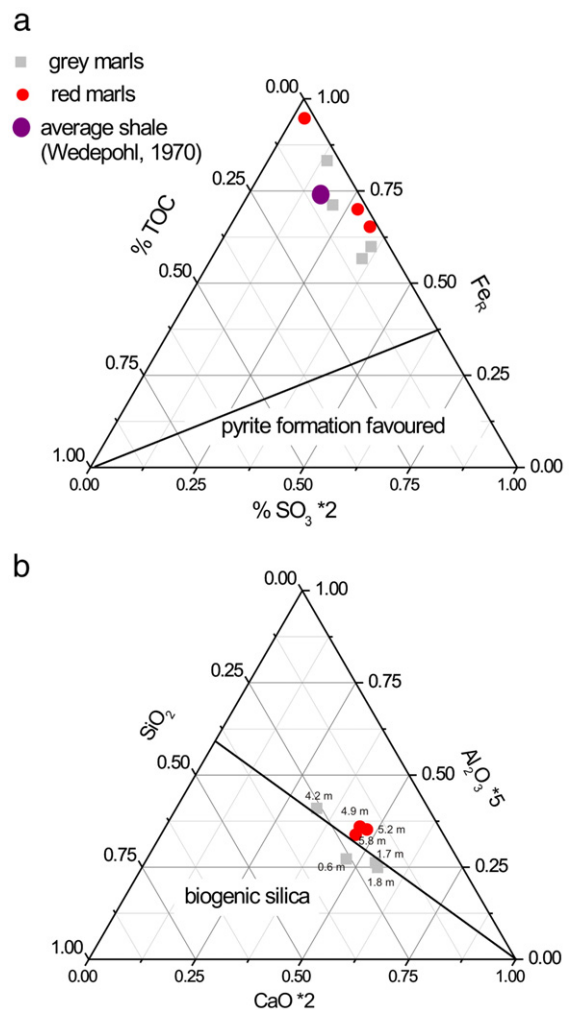


Fig. 6. Ternary diagram to determine the degree of pyritization (Brumsack, 1989), average shale value from Wedepohl (1970) (a). Ternary diagram to determine the contribution of biogenic silica to the SiO_2 budget (Rehfeld et al., 1996). Sample positions in the profile are given next to the values (b).

the shale and carbonate endmember. Clearly, most samples plot closer to the average deep-sea carbonate value. However, MnO and Na₂O in the bulk geochemical samples are significantly lower than average values. This might be caused by the pelagic source of carbonate with principally low Mg calcite. Both, K₂O and Al₂O₃ lie above a mixing line. The latter suggests a significant contribution of strongly weathered clay minerals containing Al and K in their crystal lattice (such as illite) or solely Al (such as kaolinite) (Fig. 5).

The biogenic contribution to the SiO₂ budget (Rehfeld et al., 1996) was calculated (Fig. 6a) and this identifies a significant biogenic contribution (i.e. radiolaria) in the lower part of the profile. Additionally, the degree of pyritization (DOP) was calculated following the procedure of Brumsack (1989) (Fig. 6b). The sediments experienced an early diagenetic overprint above the sulfate reduction zone, which is in accordance with no detectable pyrite (XRD).

4.4. Geochemistry of the carbonate fraction

Carbonate bound elements show no association with the carbonate content of the rocks. In general, concentrations of Ni, Co, Rb, Ti, Al, Mg, and Sr increase over the course of the profile. P lies below detection limit (below 4 µg/g) above the onset of CORB 1 and U reaches values above detection limits (0.2 µg/g) in 14 limestone samples throughout the profile.

4.5. Principal component analysis of the carbonate fraction

Prior to PCA the dataset was tested for homogeneity using CDF diagrams (Reimann et al., 2001). Due to the lithological uniformity (mostly marls and marly limestones) and to the sequential extraction of carbonates the data show a linear, continuous distribution in CDF diagrams.

Multivariate datasets such as geochemical data are frequently summarized by PCA (e.g. Reimann et al., 2001; Niebuhr, 2005). In comparison to a large set of geochemical data, PCA results in a clear summary of the main trends of a dataset. One factor summarizes a group of elements with similar trends. This can then be attributed to one or more environmental conditions. Results (PCA) from the selective leach of carbonate bound elements are summarized in Fig. 5 and described below.

4.5.1. Factor analysis

The first factor includes strong positive loadings with Ni, Sr, Ti, Mg, Al, Cd, Cu, Rb and Li (compare Fig. 7) and negative loadings with U, P, and Mn.

The three point average calculated for the depth distribution of the first factor stays fairly constant over the lower part of the profile and starts to increase at the onset of the second CORB interval (Fig. 4). High values in this factor are linked to red intervals from CORB 2 onward. Finally, factor 1 correlates negatively with δ¹³C and the SiO₂ content.

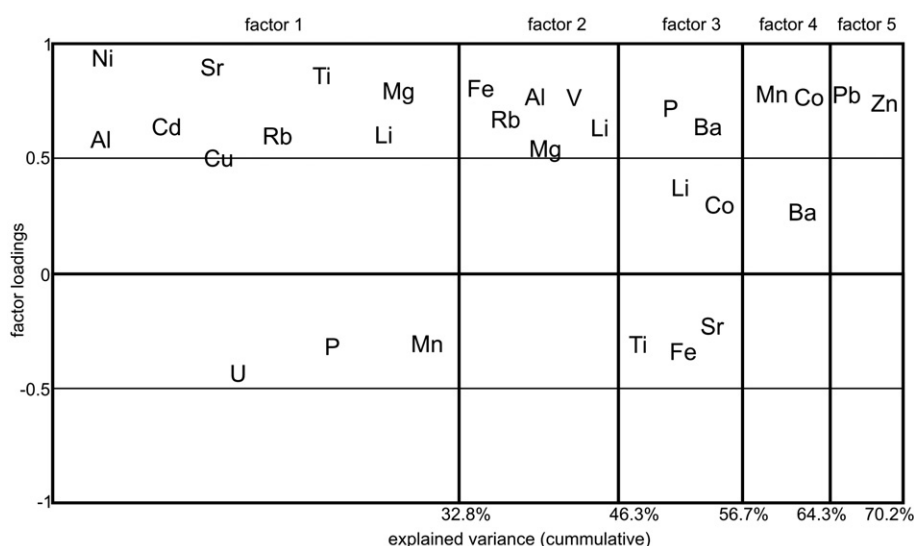


Fig. 7. Principal component analysis: factor loadings and cumulative variance explained (%). A negative loading corresponds to a negative correlation with the factor.

The second factor comprises positive loadings only (Fig. 7). This factor is uniformly distributed in the base part of the section and tends to get more variable from CORB 2 onwards (Fig. 4). The calculated three point average shows a slight increase towards CORB2 followed by a later decrease. Peaks can not be linked to any lithological changes. Finally, factor 2 correlates positively with the TOC and negatively with the phyllosilicate content.

Factor 3 comprises positive loadings with Ba and P. Other elements with weak loadings are Li and Co (Fig. 7). This factor decreases significantly (3 pt average values) below the onset of the first CORB and shows high fluctuations at the bottom of the profile (Fig. 4). Peaks at the base are mainly bound to marl layers which might indicate a dilution of the overall Ba content by increased carbonate production rates in the surface waters.

Factor 4 has positive loadings with Mn and Co and weak loading with Ba (Fig. 7). Factor 4 tends to be higher in the grey parts of the profile (Fig. 4). This factor correlates negatively with $\delta^{18}\text{O}$ (diagenesis and temperature/salinity).

The fifth factor comprises positive loadings with Zn and Pb and is highly variable (Fig. 4). This factor tends to be lower before the onset of CORB 1.

However, factor 4 and 5 are of minor importance since they explain only 8% and 6% respectively of the variances of the dataset (Fig. 7). The vast majority (32%) of the variation is explained by factor 1.

Interestingly, all factors are never coupled solely to lithological variations hence limestone and marl beds are not discernible by curves from PCA only. In addition, the slight decrease of factor 2 (Fe and V) in the red part of the profile (Fig. 4) indicates that iron oxides are

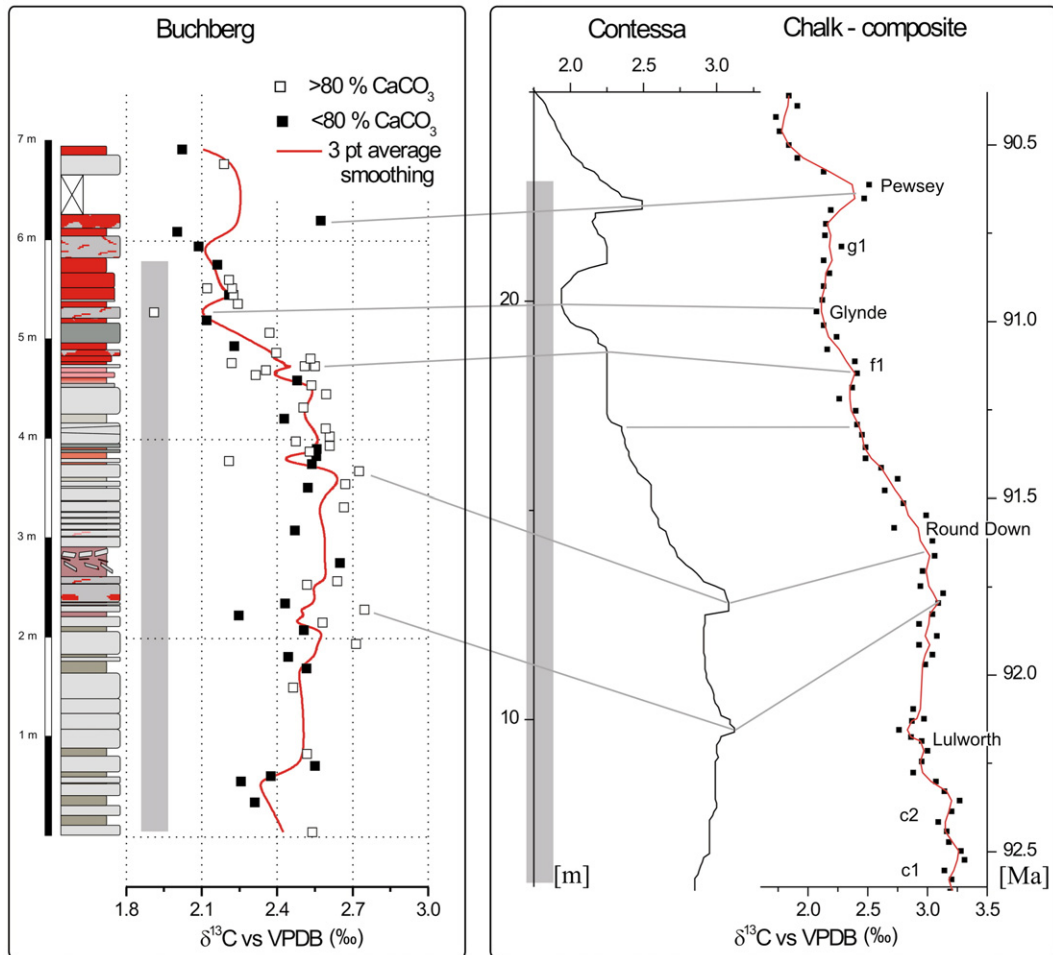


Fig. 8. Tentative correlation of Buchberg's $\delta^{13}\text{C}$ (‰) stable isotope distribution to the Contessa profile (Stoll and Schrag, 2000) and the chalk composite curve (Jarvis et al., in press). The grey bar indicates the total range zone of *H. helvetica* and correlations are based on the FO and LO datums of this marker species; bold curve: smoothed (B-spline) three point average of stable carbon isotope data.

well-crystallized and do not contribute significantly to the Fe budget in the acetate extraction. Otherwise there should be an increase in Fe instead of a decrease in these parts of the section.

4.6. Stable isotope composition

4.6.1. Carbon

The Buchberg carbon isotope profile for seawater is a three-point moving average (Fig. 8) that can be directly compared to the Tethyan Contessa profile at Gubbio (Stoll and Schrag, 2000) by correlating the Lower-Middle Turonian *H. helvetica* Zone and the nannofossil zones CC11–CC12 and UC7 and UC8. The base of the Buchberg section lies slightly above the base of the Turonian so its numerical age is projected from less than 93.5 Myr to somewhat younger than 91.0 Myr based on

the scale of Gradstein et al. (2004). The carbon isotope curve at Buchberg compares favorably with the Lower-Middle Turonian interval of the isotope curve at Gubbio and England (Jarvis et al., in press). Some of the peaks at Buchberg are defined by a single sample because of a combination of a sample spacing of 5 to 30 cm and slower sedimentation rate at Buchberg than at Contessa. Sedimentary rocks in the lower part of the *H. helvetica* Zone at Buchberg were deposited in seawater more enriched in ^{13}C than in the upper part of the Zone.

The Lower-Middle Turonian carbon isotope curve at Buchberg displays large fluctuations and has similar peaks and troughs as at Contessa (Fig. 8). Both curves show a plateau in the lower part of the *H. helvetica* Zone. In the Buchberg section the curve begins to decline slightly below 4 m and rises above 6 m. The peak at the top of the plateau and below the decline is tentatively

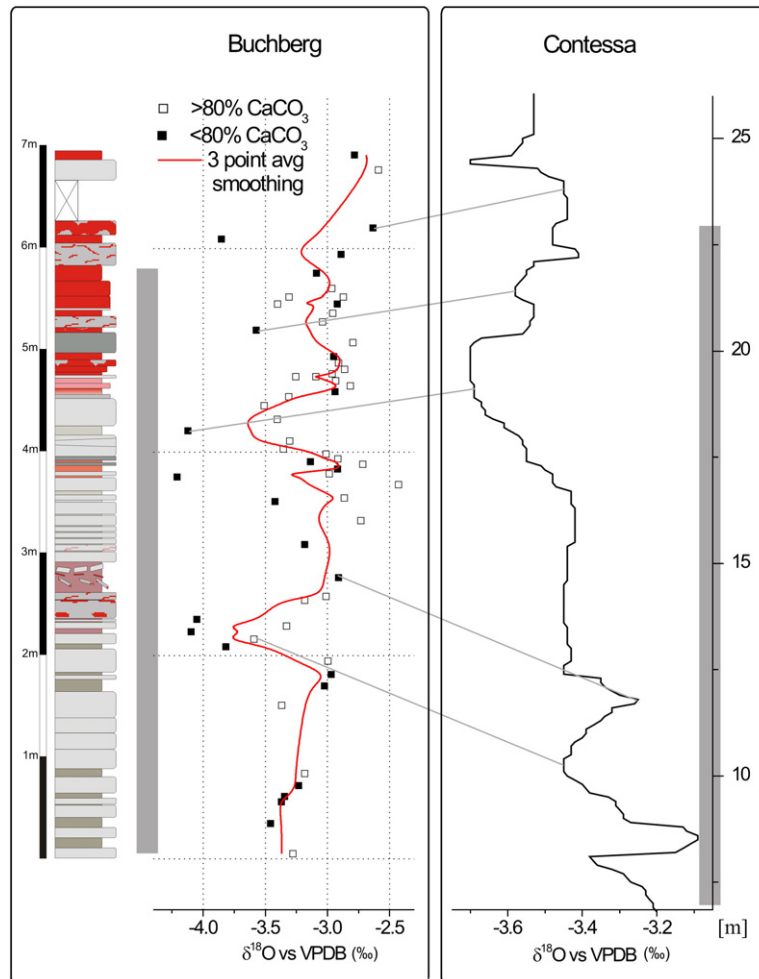


Fig. 9. Tentative correlation of Buchberg $\delta^{18}\text{O}$ (‰) stable isotope distribution and the Tethyan Contessa profile; grey bar: total range zone of *H. helvetica*; bold curve: smoothed (B-spline) tree point average of stable oxygen isotope data.

identified as the Round Down carbon isotope event (Jarvis et al., *in press*), and the low point of the curve at about 5.2 m may be the Glynde event (Fig. 8). The peak at about 6.2 m may be the Pewsey event. The magnitude of the isotope shift between the Round Down and the Glynde events at Buchberg is about 0.5‰ and at Contessa the shift is about 0.8‰. In English sections the shift is about 1‰ (Jarvis et al., *in press*).

4.6.2. Oxygen

The correlation of oxygen isotope curves between the Buchberg and Contessa section is not as straightforward as for the carbon isotopes. With the help of carbon isotope stratigraphy and the total range zone of *H. helvetica* some correlations can be attempted.

The central part of the $\delta^{18}\text{O}$ curve at Buchberg fluctuates pronouncedly. Apart from this part, increases and decreases can be correlated to Contessa (Fig. 9). In Buchberg, oxygen isotope maxima precede carbon isotope maxima. The same can be observed in the Contessa profile (Stoll and Schrag, 2000).

4.7. Stable carbon isotope stratigraphy and sediment accumulation rates

The carbon isotope events recorded in the Buchberg profile within the *H. helvetica* zone were compared to the composite curve of Jarvis et al. (*in press*) to obtain a higher resolution in age correlation as compared to biostratigraphy. Linear age–depth correlations were calculated using AnalySeries 2.0 (Paillard et al., 1996). The calibration towards an absolute timescale shows differ-

ences in the sedimentation rate between 1 and 7 mm/kyr in the profile. The absolute age by carbon isotope stratigraphy based on Jarvis et al. (*in press*) allows the calculation of the temporal extent of CORB intervals. The duration of red bed intervals varies between 30 and 360 kyrs whereas periods between CORB depositions lasted between 70 and 470 kyrs.

4.8. Diagenetic alteration

Stable isotope data do not show evidence of significant diagenetic alteration even when the samples are split in subsamples of beds above 80 and below 80% CaCO_3 . Diagenetic alteration was also examined using trace element variations (Mn/Sr vs. $\delta^{13}\text{C}$; Jacobsen and Kaufman, 1999). The CORB part was separated from the non-CORB sediments (Fig. 10a) and the dataset split into beds with carbonate content below and above 80% (Fig. 10b). According to the Mn/Sr ratio, the CORB part above 520 cm is slightly more affected by diagenesis. There is no strong relationship between Mn/Sr (i.e. degree of diagenesis) and carbonate content.

4.9. Time series analysis

Time series analyses on all data were performed using AnalySeries and PAST (<http://folk.uio.no/hammer/past/>). Both packages include a “detrend” function and a script for unevenly spaced data. Based on the correlation with the isotope curve of Jarvis et al. (*in press*) the sample depths were converted into absolute ages (see 4.7.). The shortest time step between datapoints is 10 kyr. The power

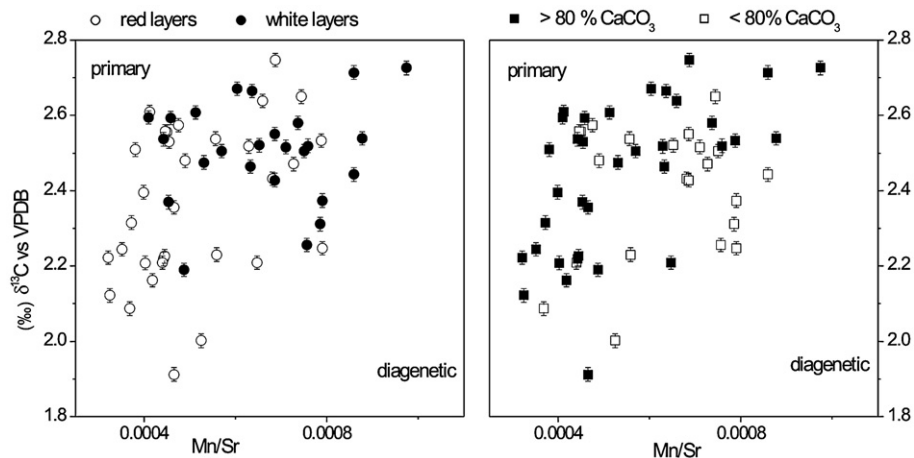


Fig. 10. Mn/Sr ratios vs. $\delta^{13}\text{C}$ (‰) to estimate the degree of diagenesis. No fractionation between red and white or grey layers can be identified (left). Some samples with carbonate content below 80% show slight diagenetic alteration (right). The five data points at the right margin correspond to marls from the base of the profile up to right below the first CORB interval.

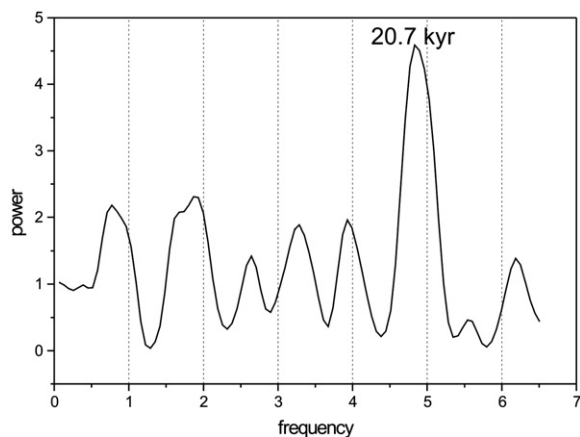


Fig. 11. Power spectrum of the carbonate content in all Buchberg samples.

spectrum of the carbonate content over the profile gave a clear peak of 20.7 kyr (Fig. 11), which corresponds to the precession cycle.

Time series analysis of the sequential extraction with acetate shows no distinct power maximum. This indicates that the variation in element geochemistry reflects chemical changes in the ocean basin and was not driven by precipitation rates of carbonate shells.

5. Discussion

The incorporation of elements in biogenic carbonate is mainly a function of its partitioning coefficient and its concentration in sea water. Sources and sinks as well as their residence times control the abundance of chemical constituents in sea water. Major sources and sinks for elements are hydrothermal processes along mid-ocean ridges as well as continental erosion and weathering due to collision and uplift (Berner and Berner, 1996). Widespread black shale deposits in the ocean can serve as source and sink by uptake and release of redox active elements as a function of the depth of the oxygen minimum zone (OMZ) (Morford and Emerson, 1999; Algeo and Maynard, 2004). Early and late diagenetic reactions may influence the elemental composition of calcitic tests as well as the composition of matrix cement.

5.1. Information from factor analysis of the acetate leach

5.1.1. Factor 1

Elements with positive loadings in factor 1 (Fig. 7) can be separated into two groups: those with a nutrient type distribution in the marine environment such as Ni,

Cd, and Cu and conservative elements like Sr, Mg, and Li. The latter get incorporated into carbonates according to their content in sea water. Further, Mg is preferably incorporated at higher temperatures (Nürnberg et al., 1996). The overall content of Mg and Rb in the ocean is governed by hydrothermal ocean floor alteration where they are depleted during periods of high hydrothermal pumping (Thompson, 1983). Sr distribution in sea water is influenced by river discharge and hydrothermal ocean basalt weathering (e.g. Veizer et al., 1999). A diagenetic decrease in Sr is accompanied by an increase in Mn (Brand and Veizer, 1980). This effect can be clearly seen in factor one (Fig. 7) with positive loadings in Sr and negative loadings in Mn.

Al extracted during the acetate leach is most likely influenced by partial dissolution of weakly crystallized Al oxides or clay minerals.

The nutrient type metals Ni and Cu are also related to hydrothermal reactions at mid-ocean ridges. Both can be released during hydrothermal venting but are thought to precipitate rapidly once they meet cold ocean waters (Thompson, 1983). The essential trace elements Ni and Cu get incorporated into organic matter (Price and Morel, 1990). The redox chemistry of Ni and incorporation into sulfides under anoxic conditions is limited due to slow reaction kinetics (Morse and Luther, 1999). Cd follows a nutrient type distribution and is mostly associated with organic matter (Bruland, 1983). It is further a redox sensitive element and gets enriched in surface sediments during suboxic diagenesis (Morford and Emerson, 1999).

Elements with negative loadings (Fig. 7) comprise redox sensitive elements (U), nutrient associated elements (P), and elements linked to diagenesis (Mn). U is transported as carbonate complex (Calvert and Pedersen, 1993) under oxic conditions. U is incorporated into suboxic sediments where it is associated with organic matter (e.g. Algeo and Maynard, 2004). A shift in bottom water oxygenation from suboxic to oxic conditions therefore stops the uptake of U into the sediment.

Acetate leaching extracts not only carbonate bound P but also P from authigenic as well as biogenic apatite (Ruttenberg, 1992). P is associated with increased surface water productivity since it is associated mainly with living tissues and is regenerated at depth during degradation of organic matter.

The main processes summarized in factor 1 are hydrothermal ocean floor basalt alteration (Rb, Mg), diagenesis (Sr, Mn), and redox signals linked to productivity (U, P).

An increase in factor 1 (Fig. 4) corresponds to a decreased hydrothermal activity where less Rb and Mg are incorporated into the basalts, a decrease in nutrient

availability (P), and most likely a change to more oxidizing bottom water conditions at sites with suboxic to anoxic diagenesis (U) such as black shale deposits. The relative enrichment in Ni and Cu might correlate with the decreased nutrient availability, which results in decreased primary production and in relative enrichment of these essential trace metals. A diagenetic contribution to factor 1 is suggested by the covariance of Mn and Sr where an increase in factor 1 suggests less diagenetic alteration (Fig. 7).

5.1.2. Factor 2

Elements linked to factor 2 are the conservative elements described in 5.1.1. as well as Fe and V (Fig. 7). Both are associated with red clays under oxic conditions (Morford and Emerson, 1999). Under slightly reducing conditions Fe and V are released into the water column and precipitate again once they meet oxygen. The transport of ferric iron may be promoted by abiotic oxidation of Fe^{2+} in the presence of organic ligands (L) forming Fe^{3+} -L complexes (Stumm et al., 1987; Luther et al., 1992). Alternatively, non-reductive dissolution of amorphous iron oxides by organic ligands may occur at circumneutral pH (Zinder et al., 1986; Luther et al., 1992). The incorporation into carbonates has to be accompanied by a reduction step. The reoxidation of V is a very slow process and V is incorporated more readily in carbonates in its reduced (VO_2^-) form (Wehrli and Stumm, 1989). Suboxic V enrichment is strongly coupled to the content of organic matter (Algeo and Maynard, 2004). Therefore depletion in factor 2 may indicate a shift towards more oxidizing conditions since less Fe and V are released into the water column but retained closer to the oxygen minimum zone (OMZ). Both elements are most likely incorporated into carbonates in discrete zones under suboxic conditions.

5.1.3. Factor 3

The positive loading of factor 3 with Ba and P (Fig. 7) is most likely a nutrient associated signal. Ba speciation in marine sediments shows that the export production of organic matter is linked to the carbonate associated Ba of samples from the equatorial Pacific (Gonneea and Paytan, 2006). Ba is linked to higher nutrient availability in seawater where barite is formed during organic matter degradation in the oxic water column (McManus et al., 1998; Babu et al., 2002) or during oxic early diagenesis (Kasten et al., 2001).

Weak positive loadings with the micronutrient Co may also be attributed phytoplankton growth (Millero and Sohn, 1992). Li is a conservative element associated with weathering, released at subduction zones and during

hydrothermal alteration of ocean floor basalts (Zhang et al., 1998).

A higher value of factor 3 most likely indicates increased nutrients and primary production in the upper water column (Fig. 4).

5.1.4. Factor 4

Mn incorporation in carbonates is a function of the oxidation state of Mn where during early diagenesis reduced Mn gets incorporated into carbonates. Compared to Fe, Mn has a slower oxidation rate (Millero et al., 1987; Thamdrup et al., 1994). This mainly indicates suboxic early diagenetic conditions where all Fe is reoxidized and Mn is retained in the carbonates. This factor is further associated with Co and a weak Ba loading (Fig. 7).

Mechanisms contributing to factor 4 can be therefore attributed to increased nutrients (Co) concomitant with increased suboxia. This conflicts with factor 1 and 3 where the upper part of the profile shows decreased nutrient availability (Fig. 4). One reason might be that primary production is limited due to lack of essential nutrients such as PO_4 (factor 3) and therefore the uptake of other trace elements (Co) is diminished.

5.1.5. Factor 5

Zn and Pb have fast precipitation kinetics with sulfide (Morse and Luther, 1999) where a higher amount of sulfate reduction decreases the availability of Pb and Zn in seawater. Under oxic conditions Pb is mostly adsorbed on particulate organic matter and Zn is incorporated into phytoplankton (Lohan et al., 2002). A positive excursion of this factor might therefore attest to a lower production of organic matter since less Pb and Zn are bound and exported to deeper settings or a decreased extent of ocean floor anoxia where less Pb and Zn are bound in the form of sulfides. The increase of factor 5 right below the first CORB (Fig. 4) might point towards the latter.

5.2. Differential diagenesis

The differentiation in carbonate and marl layers shows a slight influence of diagenetic alteration in some marl layers in the lower part of the profile (up to 2.3 m). Diagenesis may be more pronounced in limestones (e.g. Ricken, 1986). Factor 1 (Fig. 7) comprises some early diagenetic alteration especially in the grey parts of the profile. Overall, the geochemical evidence of differential diagenetic alteration is small. The reason might be that the pelagic sediments of the Ultrahelvetec continental margin are dominated by low Mg calcite tests mainly from foraminifera and coccoliths.

5.3. Nutrient distribution

Time series analysis demonstrates that carbonate production (i.e. phytoplankton blooms) follows the precession cycle (Herbert et al., 1999). This might be caused by insolation maxima or by climatic induced changes in continental runoff due to increased precipitation that results in increased input of nutrients.

Sediment accumulation rates are generally very low in this environment. Due to decomposition of organic matter during sedimentation and early diagenesis, the TOC content is not necessarily indicative of the initial TOC content and the primary production of surface waters. An entirely oxic water column most likely results in low TOC preservation with possibly high primary production in surface waters. Stable carbon isotope distribution and nutrient indicative elements (Ba, P, Cu, Ni) are used to estimate nutrient distribution. Ba and P point to higher primary production in the lower Turonian before the first CORB (Fig. 4). The Cenomanian–Turonian boundary was not recorded in the section. However, the higher content in P and Ba at the base of the section might be an aftereffect of this event. The increase in factor 1 from the second CORB onward indicates enhanced depletion of nutrients because nutrient associated elements (Cu, Ni, and Cd) are enriched at the top of the profile as a result of reduced uptake during primary production.

In general the carbonate chemistry and stable carbon isotope distribution indicates a low productive environment especially at the top of the profile. This is supported by the bulk XRF data (Fig. 5) and by the occurrence of radiolaria at the base of the profile during palaeontological screening that indicates a shift towards less biogenic silica at the top.

The sea level highstand of the Early Turonian (Gradstein et al., 2004) postdates the shift towards more oligotrophic conditions in the Buchberg section. The reworking of highly productive saltmarsh sediments in Cenomanian and Early Turonian times reported from autochthonous Cretaceous deposits on the Bohemian Massif (Fuchs et al., 1984) is one possible source of nutrients before the onset of the oligotrophic conditions.

5.4. Element cycling and redox conditions of the Middle Turonian in the Ultrahelvetic realm

During episodes of changing redox conditions black shales can act both as sources and sinks of elements associated with sulfides and organic matter. For example, a release of elements from widespread black shale deposited at the southern margin of the Tethys, in

the central Tethyan troughs (for a summary see Luning et al., 2004), and in the Atlantic (Kuhnt et al., 1997) could have enriched redox active elements in the surface ocean which were incorporated into foraminiferal and nannofossil tests (Morford and Emerson, 1999) as described by factor one and five (Fig. 4). In the same way elements can have been removed from the ocean system by drawdown due to increased anoxia as proposed for Devonian black shales (Algeo and Maynard, 2004).

V and Fe (factor 2) may originate from areas above the OMZ in adjacent basins, which are highly influenced by a subtle shift of the OMZ. Fe and V get enriched above the OMZ by reductive dissolution followed by reoxidation at the onset of the oxic zone. An upward shift of the OMZ releases these elements into the water column.

The increase in factor 5 (Pb and Zn) before the first CORB interval (Fig. 4) indicates a shift towards more oxygenated bottom waters where less Pb and Zn is bound in sulfidic sediments.

The onset of the second CORB interval, which is tentatively correlated to the Round Down carbon isotope event (Fig. 8) of Jarvis et al. (in press), is accompanied by an increase in factor 1 and a maximum in factor 2 (Fig. 4). This points towards a higher oxygen concentration in the bottom waters during deposition of the upper part of the profile also suggested by decreased U concentrations. The maxima of factor 1 in CORBs indicate that CORB intervals were more oligotrophic as compared to sediments beneath and above.

A higher bottom water oxygen content displayed in factor 1 can probably be attributed to a change in ocean circulation since it is unlikely that the large sources of black shales ran out of U after the Round Down carbon isotope event. Possibly in this part of the Tethys a shift in ocean circulation resulted in a generally more oxic environment.

The stable carbon isotope values (Fig. 8) indicate that sediments in the lower *H. helvetica* zone were deposited in seawater enriched in ¹³C compared to the upper *H. helvetica* zone. This also points towards more oligotrophic surface ocean conditions.

5.5. Hydrothermal ocean floor alteration

Interaction between ocean bottom water and hot basalts at mid-ocean ridges is a significant mechanism for the distribution of conservative elements in ocean basins (Thompson, 1983; Millero and Sohn, 1992). The closest possible sources of hydrothermal fluids were the spreading center of the Alpine Tethys or the branch of the Tethys to the south of the Alpine terrane (Fig. 1). Factor 1 and 2 show the strongest loadings with conservative elements associated with basalt-seawater

interaction (Fig. 7). An increase in both factors indicates a decrease in hydrothermal ocean floor alteration with an increase of Mg and Rb in the ocean. The maximum value at the onset of CORB 2 (Fig. 4) points towards a minimum of hydrothermal venting at mid-ocean ridges and the gradual increase of Factor 1 above the Round Down isotope event might partly be attributed to decreased ocean floor spreading rate.

5.6. Formation of CORBs

CORBs owe their colour to finely dispersed hematite and to hematite-encrusted grains. The origin and enrichment mechanisms of hematite during marine red bed formation has been strongly discussed during the past decades (Franke and Paul, 1980; Eren and Kadir, 1999). The main issue of debate is the mechanism of iron enrichment during red bed formation because diagenetic iron enrichment requires a reductive step. The other possible source is iron oxide import from oxidized lateritic soils. In the Buchberg profile, the colouring is initially bound to layers with higher phyllosilicate content with less dilution by biogenic carbonate. Farther upward in the profile the colouring by iron oxides affects limestones as well. Visibly, the oxidation of iron is enlarged in CORBs. In bulk geochemical analyses, the total Fe content correlates strongly with Al ($R=0.95$). Therefore the source of Fe is mainly related to the terrigenous fraction namely smectitic clay minerals (Franke and Paul, 1980) with easily exchangeable interstitial cations or iron oxides associated with those clays (Bensing et al., 2005). Carbonate bound iron does not follow a particular pattern even though it is enriched in grey limestones associated with CORB3 (Fig. 4). The incorporation of iron into carbonates requires a reductive step where iron is mobilized and is bound in the carbonate lattice as ferrous cation. For CORB3 the hematite enrichment could be explained by more suboxic conditions during limestone deposition with an increased early diagenetic incorporation of ferrous iron. Parts of Fe might get mobilized during early diagenesis and re-precipitate once they meet more oxic marl beds. Reduction in limestones most likely does not occur as an oxidation front but in discrete zones with a lower Eh due to inhomogeneities in initial TOC content on small scale.

The sedimentation of CORBs seems to be independent of orbital variations and was therefore not primarily linked to changes in the carbonate production rate in surface waters. Factor 1 is linked to CORB formation from the second CORB interval onward where essential trace metals (Ni, Cu) are enriched during CORB times

(Fig. 4). These periods most likely correspond to times of reduced hydrothermal venting. Most likely the depletion of essential nutrients such as P or Fe resulted in a lower primary production during CORB times. One likely nutrient is P, which is limiting in most parts of today's ocean and P values are below detection limit above CORB1. Since nutrient type metals (Ni, Cu) and conservative metals (Mg, Rb) covary in factor 1 it is speculated that hydrothermal activity at mid-ocean ridges is an additional source of certain trace metals. Higher Mn values in grey beds are most likely associated with suboxic early diagenesis (see factor 4, Fig. 4). This could indicate that periods between CORBs have slightly increased primary production.

6. Conclusion

This study shows that the Early and Middle Turonian was a time period of oligotrophic conditions in the Ultrahelvetic realm. A gradual nutrient depletion (most likely phosphate depletion in the surface waters) during this time interval resulted in enhanced oligotrophy, which ultimately lead to the formation of CORBs. From the onset of the first red bed a decreased availability of nutrients (P), nutrient indicative trace elements (Ba), and an increase in bottom water oxygenation (Pb, Zn) in basins with black shale deposits can be seen. Overall, the depth of the oxygen minimum zone in adjacent basins (Atlantic or southern part of the Tethys ocean) increased during this time period.

We identified a precessional (20 kyr) forcing on primary production represented by the total carbonate content. This low productive environment can be correlated biostratigraphically and by stable isotope stratigraphy to dated profiles from the European shelf (Jarvis et al., *in press*). This constrains the duration of individual CORB depositional events to between 30 and 360 kyrs.

The Round Down stable isotope event is coeval with the transition of declined primary production and reduced hydrothermal ocean floor alteration as suggested by the carbonate geochemical composition.

Acknowledgements

S.N. was supported by a DocFForte grant for PhD students of the Austrian Academy of Sciences. Field work was covered by IGCP 494 grants of the Austrian Academy of Sciences. We are grateful for the help of Wilfried Körner, Andreas Doll (both: Dept. of Environmental Geosciences, University of Vienna), and Manuela Wimmer (Institute of Geology and Paleontology, University of Innsbruck) with ICP-MS and stable isotope

measurements. Susanne Gier (Department of Geodynamics and Sedimentology, Univ. Vienna) and Franz Ottner (Dept. Applied Geosciences, Univ. of Natural Resources and Applied Life Sciences, Vienna) provided their clay mineralogical expertise.

Thomas Neumann (Dept. of Mineralogy and Geochemistry, Univ. Karlsruhe) is acknowledged for discussion of the manuscript. We thank Robert W. Scott, and two anonymous scientists for their thoughtful reviews and Finn Surlyk for editing the manuscript. This is a contribution to the IGCP projects 494 and 463.

Appendix A. Supplementary data

Supplementary data associated with this article can be found, in the online version, at [doi:10.1016/j.palaeo.2007.03.049](https://doi.org/10.1016/j.palaeo.2007.03.049).

References

- Algeo, T.J., Maynard, J.B., 2004. Trace-element behavior and redox facies in core shales of Upper Pennsylvanian Kansas-type cyclothems. *Chem. Geol.* 206, 289–318.
- Babu, C.P., Brumsack, H.J., Schmetger, B., Bottcher, M.E., 2002. Barium as a productivity proxy in continental margin sediments: a study from the eastern Arabian Sea. *Mar. Geol.* 184, 189–206.
- Bensing, J.P., Mozley, P.S., Dunbar, N.W., 2005. Importance of clay in iron transport and sediment reddening: evidence from reduction features of the ABO Formation, New Mexico, USA. *J. Sediment Res.* 75, 562–571.
- Berner, E.K., Berner, R.A., 1996. *The Global Environment: Water, Air, and Geochemical Cycles*. Prentice–Hall, Upper Saddle River, NJ. 376 pp.
- Brand, U., Veizer, J., 1980. Chemical diagenesis of a multicomponent carbonate system. I. Trace-elements. *J. Sediment Petrol.* 50, 1219–1236.
- Bruland, K.W., 1983. Trace elements in sea water, In: Riley, J.P., Chester, R. (Eds.), *Chemical Oceanography*, second ed. Academic Press, London, pp. 147–220.
- Brumsack, H.J., 1989. Geochemistry of recent TOC-rich sediments from the Gulf of California and the Black-Sea. *Geol. Rundsch.* 78, 851–882.
- Burnett, J.A., Gallagher, L.T., Hampton, M.J., 1989. Upper Cretaceous. In: Brown, P.R. (Ed.), *Calcareous Nannofossil Biostratigraphy*. Chapman and Hall, London, pp. 132–199.
- Calvert, S.E., Pedersen, T.F., 1993. Geochemistry of recent oxic and anoxic marine-sediments — implications for the geological record. *Mar. Geol.* 113, 67–88.
- Eren, M., Kadir, S., 1999. Colour origin of upper cretaceous pelagic red sediments within the Eastern Pontides, northeast Turkey. *Int. J. Earth Sci.* 80, 593–595.
- Faupl, P., Wagreich, M., 2000. Late Jurassic to Eocene palaeogeography and geodynamic evolution of the Eastern Alps. *Mitt. Österr. Geol. Ges.* 92, 79–94.
- Franke, W., Paul, J., 1980. Pelagic redbeds in the Devonian of German — deposition and diagenesis. *Sediment. Geol.* 25, 231–256.
- Fuchs, R., Wessely, G., Schreiber, O.S., 1984. The Middle and Upper Cretaceous underlying the Molasse along the Southern extension of the Bohemian Massif. *Schriften. Erdwiss. Komm.* 7, 193–220.
- Gradstein, F.M., Ogg, J.G., Smith, A.G., 2004. *A Geologic Time Scale*. Cambridge University Press, Cambridge. 589 pp.
- Gonneea, M.E., Paytan, A., 2006. Phase associations of barium in marine sediments. *Mar. Chem.* 100, 124–135.
- Herbert, T.D., Gee, J., DiDonna, S., 1999. Precessional cycles in Upper Cretaceous pelagic sediments of the South Atlantic: long-term patterns from high-frequency climate variations. In: Barrera, E., Johnson, C.C. (Eds.), *Evolution of the Cretaceous Ocean–Climate System*. Geological Society of America Special Paper, vol. 332, pp. 105–120.
- Hoelzel, M., 2004. StratDraw: automatic generation of stratigraphic sections from tabulated field data. *Comput. Geosci.* 30, 785–789.
- Hu, X.M., Jansa, L., Wang, C.S., Sarti, M., Bak, K., Wagreich, M., Michalik, J., Sotak, J., 2005a. Upper Cretaceous oceanic red beds (CORBs) in the Tethys: occurrences, lithofacies, age, and environments. *Cretac. Res.* 26, 3–20.
- Hu, X., Jansa, L., Sarti, M., 2005b. Mid-Cretaceous oceanic red beds in the Umbria-Marche Basin, central Italy: constraints on paleoceanography and paleoclimate. *Palaeogeography, Palaeoclimatology, Palaeoecology* 233, 163–186.
- Jacobsen, S.B., Kaufman, A.J., 1999. The Sr, C and O isotopic evolution of Neoproterozoic seawater. *Chem. Geol.* 161, 37–57.
- Jarvis, I., Gale, A.S., Jekyns, H.C., Pearce, M., in press. Secular variation in Late Cretaceous carbon isotopes: a new $\delta^{13}\text{C}$ carbonate reference curve for the Cenomanian–Campanian (99.6–70.6 Ma). *Geol. Mag.*
- Kasten, S., Haese, R.R., Zabel, M., Ruhlemann, C., Schulz, H.D., 2001. Barium peaks at glacial terminations in sediments of the equatorial Atlantic Ocean — relicts of deglacial productivity pulses? *Chem. Geol.* 175, 635–651.
- Kuht, W., Nederbragt, A., Leine, L., 1997. Cyclicity of Cenomanian–Turonian organic-carbon-rich sediments in the Tarfaya Atlantic Coastal Basin (Morocco). *Cretac. Res.* 18, 587–601.
- Lohan, M.C., Statham, P.J., Crawford, D.W., 2002. Total dissolved zinc in the upper water column of the subarctic North East Pacific. *Deep-Sea Res.* 2, 5793–5808.
- Luning, S., Kolonic, S., Belhadj, E.M., Belhadj, Z., Cota, L., Baric, G., Wagner, T., 2004. Integrated depositional model for the Cenomanian–Turonian organic-rich strata in North Africa. *Earth-Sci. Rev.* 64, 51–117.
- Luther, G.W., Kostka, J.E., Church, T.M., Sulzberger, B., Stumm, W., 1992. Seasonal iron cycling in the Salt-Marsh sedimentary environment — the importance of ligand complexes with Fe(II) and Fe(III) in the dissolution of Fe(III) minerals and pyrite, respectively. *Mar. Chem.* 40, 81–103.
- McManus, J., Berelson, W.M., Klinkhammer, G.P., Johnson, K.S., Coale, K.H., Anderson, R.F., Kumar, N., Burdige, D.J., Hammond, D.E., Brumsack, H.J., McCorkle, D.C., Rushdi, A., 1998. Geochemistry of barium in marine sediments: implications for its use as a paleoproxy. *Geochim. Cosmochim. Acta* 62, 3453–3473.
- Melim, L.A., Westphal, H., Swart, P.K., Eberli, G.P., Munnecke, A., 2002. Questioning carbonate diagenetic paradigms: evidence from the Neogene of the Bahamas. *Mar. Geol.* 185, 27–53.
- Melinte, M.C., Jipa, D., 2005. Campanian–Maastrichtian marine red beds in Romania: biostratigraphic and genetic significance. *Cretac. Res.* 26, 49–56.
- Millero, F.J., Sohn, M.L., 1992. *Chemical Oceanography*. CRC Press, Boca Raton. 531 pp.
- Millero, F.J., Sotolongo, S., Izaguirre, M., 1987. The oxidation-kinetics of Fe(II) in seawater. *Geochim. Cosmochim. Acta* 51, 793–801.

- Morford, J.L., Emerson, S., 1999. The geochemistry of redox sensitive trace metals in sediments. *Geochim. Cosmochim. Acta* 63, 1735–1750.
- Morse, J.W., Luther, G.W., 1999. Chemical influences on trace metal–sulfide interactions in anoxic sediments. *Geochim. Cosmochim. Acta* 63, 3373–3378.
- Niebuhr, B., 2005. Geochemistry and time-series analyses of orbitally forced Upper Cretaceous marl–limestone rhythmites (Lehrte West Syncline, northern Germany). *Geol. Mag.* 142, 31–55.
- Nürnberg, D., Bijma, J., Hemleben, C., 1996. Assessing the reliability of magnesium in foraminiferal calcite as a proxy for water mass temperatures. *Geochim. Cosmochim. Acta* 60, 803–814.
- ÖNORM L1084 Chemische Bodenuntersuchung - Bestimmung von Carbonat.
- Paillard, D., Labeyrie, L., Yiou, P., 1996. Macintosh program performs time series analysis. *Eos, Trans. – Am. Geophys. Union* 77, 379.
- Perch-Nielsen, K., 1985. Mesozoic Calcareous Nannofossils. In: Bolli, H.M., Saunders, J.B., Perch-Nielsen, K. (Eds.), *Plankton Stratigraphy*. Cambridge University Press, Cambridge, pp. 329–426.
- Poulsen, C.J., Seidov, D., Barron, E.J., Peterson, W.H., 1998. The impact of palaeogeographic evolution on the surface oceanic circulation and the marine environment within the mid-Cretaceous Tethys. *Paleoceanography* 13, 546–559.
- Price, N.M., Morel, F.M.M., 1990. Cadmium and cobalt substitution for zinc in a marine diatom. *Nature* 344, 658–660.
- Puceat, E., Lecuyer, C., Reisberg, L., 2005. Neodymium isotope evolution of NW Tethyan upper ocean waters throughout the Cretaceous. *Earth Planet. Sci. Lett.* 236, 705–720.
- Rehfeld, U., Niebuhr, B., Ernst, G., 1996. Sedimentology, geochemistry and faunal distribution triggered by orbital forcing in an Upper Campanian marl–limestone succession of N-Germany (Misburg/Hannover, Lower Saxony Basin). *Zentralblatt für Geologie und Paläontologie* 1 (11–12), 1263–1292.
- Reimann, C., Filzmoser, P., Garrett, R.G., 2001. Factor analysis applied to regional geochemical data: problems and possibilities. *Appl. Geochem.* 17, 185–206.
- Ricken, W., 1986. Diagenetic bedding: a model for Limestone–Marl alternations. *Lect. Notes Earth Sci.*, vol. 6. Springer, Berlin.
- Ruttenberg, K.C., 1992. Development of a sequential extraction method for different forms of phosphorus in marine-sediments. *Limnol. Oceanogr.* 37, 1460–1482.
- Schultz, L.G., 1964. Quantitative interpretation of mineralogical composition from X-ray and chemical data for the Rierre shale. *US Geol. Survey Prof Paper*, vol. 391.
- Spötl, C., Vennemann, T., 2003. Continuous-flow isotope ratio mass spectrometric analysis of carbonite minerals. *Rapid Commun. Mass Spectrom.* 17, 1004–1006.
- Stampfli, G.M., Borel, G., Marchant, R., Mosar, J., 2002. Western Alps geological constraints on western Tethyan reconstructions. *J. Virtual Explor.* 8, 77–106.
- Stoll, H.M., Schrag, D.P., 2000. High-resolution stable isotope records from the Upper Cretaceous rocks of Italy and Spain: glacial episodes in a greenhouse planet? *Geol. Soc. Amer. Bull.* 112, 308–319.
- Stumm, W., Wehrli, B., Wieland, E., 1987. Surface complexation and its impact on geochemical kinetics. *Croat. Chem. Acta* 60, 429–456.
- Sulkowski, M., Hirner, A.V., 2006. Element fractionation by sequential extraction in a soil with high carbonate content. *Appl. Geochem.* 21, 16–28.
- Tessier, A., Campbell, P.G.C., Bisson, M., 1979. Sequential extraction procedure for the speciation of particulate trace-metals. *Anal. Chem.* 51, 844–851.
- Thamdrup, B., Glud, R.N., Hansen, J.W., 1994. Manganese oxidation and in-situ manganese fluxes from a coastal sediment. *Geochim. Cosmochim. Acta* 58, 2563–2570.
- Thompson, G., 1983. Basalt–seawater interaction. In: Rona, P.A., Boström, K., Laubier, L., Smith Jr. K.L. (Eds.), *Hydrothermal Processes at Seafloor Spreading Centers*. Plenum Press, New York, pp. 225–278.
- Turekian, K.K., Wedepohl, K.H., 1961. Distribution of the elements in some major units of the Earth's crust. *Geol. Soc. Am. Bull.* 72, 175–191.
- Tyrrell, T., Zeebe, R.E., 2004. History of carbonate ion concentration over the last 100 million years. *Geochim. Cosmochim. Acta* 68, 3521–3530.
- Veizer, J., Ala, D., Azmy, K., Bruckschen, P., Buhl, D., Bruhn, F., Carden, G.A.F., Diener, A., Ebner, S., Godderis, Y., Jasper, T., Korte, C., Pawellek, F., Podlaha, O.G., Strauss, H., 1999. Sr-87/Sr-86, delta C-13 and delta O-18 evolution of Phanerozoic seawater. *Chem. Geol.* 161, 59–88.
- Wang, C.S., Hu, X., 2005. Cretaceous world and oceanic red beds. *Earth Sci. Front.* 12, 11–21.
- Wang, C.S., Hu, X.M., Sarti, M., Scott, R.W., Li, X.H.M., 2005. Upper Cretaceous oceanic red beds in southern Tibet: a major change from anoxic to oxic, deep-sea environments. *Cretac. Res.* 26, 21–32.
- Wehrli, B., Stumm, W., 1989. Vanadyl in natural-waters — adsorption and hydrolysis promote oxygenation. *Geochim. Cosmochim. Acta* 53, 69–77.
- Zhang, L.B., Chan, L.H., Chan, L.H., Gieskes, J.M., 1998. Lithium isotope geochemistry of pore waters from Ocean Drilling Program Sites 918 and 919, Irminger Basin. *Geochim. Cosmochim. Acta* 62, 2437–2450.
- Zinder, B., Furrer, G., Stumm, W., 1986. The coordination chemistry of weathering 2. Dissolution of Fe(III) Oxides. *Geochim. Cosmochim. Acta* 50, 1861–1869.